

Quantitative Morphology of Moderate Redshift Galaxies :
How Many Peculiars Are There ?

Avi Naim, Kavan U. Ratnatunga AND Richard E. Griffiths

The Johns Hopkins University, Department of Physics & Astronomy,
Baltimore, MD 21218, U.S.A.¹

¹ current address : Physics Department, Wean Hall, Carnegie Mellon University,
5000 Forbes Avenue, Pittsburgh, PA 15213

Received _____; accepted _____

ABSTRACT

The advent of the Hubble Space Telescope (HST) has provided images of galaxies at moderate and high redshifts and changed the scope of galaxy morphologies considerably. It is evident that the Hubble Sequence requires modifications in order to incorporate all the various morphologies one encounters at such redshifts. We investigate and compare different approaches to quantifying peculiar galaxy morphologies on images obtained from the Medium Deep Survey (MDS) and other surveys using the Wide Field Planetary Camera 2 (WFPC2) on board the HST, in the I band (filter F814W). We define criteria for peculiarity and put them to use on a sample of 978 galaxies, classifying them by eye as either normal or peculiar. Based on our criteria and on concepts borrowed from digital image processing we design a set of four purely morphological parameters, which comprise the overall texture (or “blobbiness”) of the image; the distortion of isophotes; the filling-factor of isophotes; and the skeleta of detected structures. We also examine the parameters suggested by Abraham *et al.* (1995). An artificial neural network (ANN) is trained to distinguish between normal and peculiar galaxies. While the majority of peculiar galaxies are disk-dominated, we also find evidence for a significant population of bulge-dominated peculiars. Consequently, peculiar galaxies do not all form a “natural” continuation of the Hubble sequence beyond the late spirals and the irregulars. The trained neural network is applied to a second, larger sample of 1999 WFPC2 images and its probabilistic capabilities are used to estimate the frequency of peculiar galaxies at moderate redshifts as $35 \pm 15\%$.

Subject headings: galaxies: morphology - galaxies: evolution - galaxies: peculiar

1. Introduction

The Hubble Sequence (Hubble 1936) and its revisions (e.g., Sandage 1961; de Vaucouleurs *et al.* 1959; van den Bergh 1976) all address the local universe, in effect defining the mainstream of “normal” galaxies. It has been known for a long time that some galaxies do not fit in these schemes. Arp (1966) published an atlas of *peculiar* galaxies which shows an impressive variety of morphologies deemed “strange” or “interesting”. However, quantifying the notion of peculiarity is still a challenge. This may be partly due to the fact that peculiar galaxies were regarded as rare exceptions unrelated to each other, rather than a coherent class (or classes) of galaxies.

The advent of the Hubble Space Telescope (HST) has allowed us to view the universe of galaxies in much greater depth than ever before. Images in parallel mode from fields of the Medium Deep Survey (MDS) key project and other observations give us a first look at large numbers of galaxies residing at moderate redshifts. The galaxy population at a redshift of about 0.5 looks quite different from that of the local universe : A significant population of blue irregular galaxies was reported (Griffiths *et al.* 1994) which appears to account for much of the increase in number counts at faint magnitudes (Glazebrook *et al.* 1995; Driver *et al.* 1995). In addition, the incidence of morphological peculiarities among these galaxies appears to be higher than in nearby galaxies (e.g., Abraham *et al.* 1995, hereafter A95). Further out at redshifts exceeding 1 a new morphological class, called “chain galaxies”, was recently reported by Cowie *et al.* (1995), although their nature has already been disputed (Dalcanton & Smetman 1996). An inherent problem of such observations is that the rest frame of the observed band is shifted bluewards with increasing redshift. It is difficult to quantify the effect of this shift on the observed images. We discuss below the effect of observing moderate redshift galaxies in the V band (filter F606W) as compared with the I band (F814W). Nevertheless, even without accounting for the shift in rest frame band it appears that the Hubble Sequence needs to be extended or replaced by a more general scheme in order to accommodate the diversity of shape found among moderate redshift galaxies.

The numbers clearly show that peculiar galaxies can no longer be regarded as rare exceptions.

So far, most published work in this field quoted numbers based on eyeball classification of HST images. However, as was pointed out by Lahav & Naim (1996), this approach suffers from two major problems : First, the notion of morphological peculiarity is not well defined. There is little agreement - even among experts - on what qualifies as a peculiar galaxy. As a result it is very difficult to compare results from papers by different authors, and in particular a wide range of values are given for the fraction of peculiar galaxies at moderate redshifts. A second, related problem is the difficulty in obtaining consistent eyeball classifications for large quantities of galaxies. A95 realised these problems and took the important first step of introducing a quantitative measure of peculiarity which can be used to automatically classify galaxies.

In this paper we answer two related, yet separate, questions : First, how can one “teach” a computer to tell whether a given galaxy is peculiar or not (given an accepted definition for peculiarity). Second, what is the fraction of peculiar galaxies at moderate redshifts in the universe. Our premise is that quantitative measures are crucial if one is to standardise the concept of peculiar galaxies. We seek to put this quantitative distinction on firm grounds. Since the notion of peculiarity is not well defined we begin in § 2 by describing the galaxy samples and discussing our criteria in the light of several examples for various types of peculiarity. In § 3 we translate our criteria to four quantitative parameters (hereafter the “4P-set”) and show through examples how they are measured. In § 4 we train *Artificial Neural Networks* (ANNs) to distinguish between normal and peculiar galaxies. We compare the A95 set of parameters (hereafter the “C-A set”) to the 4P set by training three different ANNs. In § 5 we study the limitations of our parameters and examine the ANN success rates as a function of magnitude, signal-to-noise ratio and image size, below which our method breaks down. We then use the trained ANN to classify a larger set of images,

for which no eyeball classification is available. In § 6 we examine the frequency of peculiarity as a function of the relative importance of the bulge, in an attempt to determine whether peculiar galaxies are all disk-dominated. The discussion follows in § 7.

2. Galaxy Samples and Criteria for Peculiarity

2.1. Galaxy Samples

Our “sample 1” consists of some 1059 images in 9 Groth-Westphal strip fields (Groth *et al.* 1995), and is complete down to a limiting isophotal magnitude of 24.0 in the I band (filter F814W). Of these, 81 are rejected either because they are identified by eye as stars or point sources or due to low picture quality (e.g., too many bad pixels). The remaining 978 images are deemed galaxies. Once the ANN is trained we apply it to the rest of the Groth-Westphal strip, down to $I = 24.0$. This larger “sample 2” contains 2319 images in 18 more fields. One problem with sample 2 is that it contains stars as well as galaxies, and we need a quantitative criterion for identifying them. We discuss such a criterion below.

2.2. A Qualitative Discussion of Criteria for Peculiarity

A peculiar galaxy is most easily characterised as any galaxy that is not morphologically “normal”. This, in turn, suggests using a representative set of normal galaxies as templates and comparing any given image to this entire set. One would then expect the more extreme peculiars to stand out as very dissimilar to any of the templates. However, such an approach has already been tried without much success by Lahav & Naim (1996), and they conclude that rather than use the whole image as a template one should look for certain important *features*, those which change the

most between normal and peculiar galaxies.

In figure 1 we show twelve examples of I band images, taken from sample 1. The top nine of these show galaxies with various peculiar features and the bottom three look normal. The peculiar features of the top nine are (going left to right, then top to bottom) : Very bright “knots” on an otherwise quiet background; a polar ring galaxy; an apparent merger of two galaxies; a weird overall shape; an asymmetric shape; a double core (or an ongoing merger); a “knot” at the end of an edge-on disk; faint spiral arms going in two different senses; an arc on one side of the bulge only. Some of these features are not easy to see in the printed version of the images. From an examination of these and other images in sample 1 we came up with two characteristics of peculiarity :

1. The nature of bright, localised structure : Many galaxies are considered peculiar due to the existence of very bright, round features (e.g., “knots”), as opposed to elongated arms or arm fragments in spirals.
2. The degree of symmetry of the image : A different kind of peculiarity is an asymmetric shape. In some cases the asymmetry affects the fainter isophotes (e.g., tidal tails), while in others the shape of the image as a whole is rather symmetric, but superposed on it are bright asymmetric features.

2.3. Eyeball Classifications

The images were examined in the I (F814W) and V (F606W) bands *separately* by one of us (AN) on a computer screen, and assigned one of the following morphological classes : E/S0; Se; Sl; P1; P2. “Se” stands for early type spirals and includes all types in the range S0/a to Sbc. “Sl” stands for late type spirals, and includes all types from Sc through to Im. A distinction between two general types of peculiarity is also made : Galaxies with a distorted shape are assigned type “P1”, while those that

exhibit localised features (e.g., bright “knots”) are assigned type “P2”. If a galaxy qualifies as peculiar on both counts, the assigned type is “P2”. The galaxies in the first three bins are collectively labeled “normal” and those in the latter two are labeled “peculiar”. We would like to point out that there is some confusion in the literature between “Irregular” and “Peculiar” galaxies. We define Irregulars as disk dominated galaxies with a small or no bulge component, and a fairly flat intensity profile, thus lumping together in this class the revised Hubble types Sdm, Sm and Im. Irregulars are therefore normal galaxies as far as this paper is concerned and belong to the “SI” bin described above. On the other hand, for a galaxy to be labeled as peculiar at least one of the criteria we specify above has to be met. Such galaxies can not be assigned Hubble types by definition, although they may resemble normal galaxies in some respects.

The approach adopted here is very liberal towards peculiars : even the slightest distortions or a single faint knot are enough for a classification as a peculiar. This means that galaxies that appear normal but for some small feature are also called peculiar in our sample. We would like to emphasise that regardless of the criteria employed, the morphologies of galaxies form sequences, and where one draws the line between one type and another is always subjective. In recognition of the many border line cases (especially at the faint end), each peculiar galaxy is also assigned a certainty index, stating simply if its “peculiar” tag is certain or uncertain. The distribution of sample 1 galaxies among the classes is shown in table 1 below.

Some 62% of the galaxies receive exactly the same classification, and the I and V classifications of 80% differ by no more than one type within each general (normal/peculiar) class. However, there is a “migration” of galaxies from earlier and normal types in I to later and peculiar types in V. This can be seen from the much higher number of galaxies above the diagonal in table 1 (297), compared with the number of galaxies below the diagonal (78). This trend entails a significant increase in the number of peculiars detected in V. One possible explanation for this effect is

that in the range of redshifts covered by our samples (the median redshift of galaxies down to $I \sim 22$ is about 0.6) the V filter corresponds to a band that is *bluer* than the rest-frame B band, while the I filter corresponds to a band slightly redder than B in the rest frame. Practically all the existing classification schemes for galaxies were defined in the B band for relatively nearby galaxies. In the local universe the reliability of eyeball classification deteriorates fast as one goes bluer than B, and UV morphologies can look very odd compared to their B counterparts. Many of the images in our samples are fainter than $I \sim 22$, which implies an even higher redshift than 0.6 and consequently an even bluer pass band. Ideally, one would wish to have a classification scheme for all images in the same rest wavelength, but in practice this is impossible. On top of this problem, in the Groth-Westphal strip the V band exposures were about 30% shorter than the I band exposures. As a result many images in the V band suffer from lower signal-to-noise ratio, which contributes the spurious structure and in general misleads the eye to "see" more fragmented structure and smaller bulges. Overall, 306 galaxies (31% of sample 1) are assigned peculiar types in the I band and 432 galaxies (44% of sample 1) are assigned peculiar types in the V band.

3. Quantitative Parameters for Peculiarity

Following the discussion above, we adopt the I band images for training the ANN. All of the parameters described below are derived for I band images. The images are first treated with a reduction and fitting software written by one of us (KUR), which performs a maximum-likelihood analysis of the full 2-dimensional image in order to simultaneously fit the sky level, the image center, size, position angle and axis ratio, and determine the best fitting photometric model (bulge, disk or bulge+disk; see Ratnatunga *et al.*, *in preparation* for full details). The original images are used for calculating the C-A set of A95. In calculating our 4P set we use both the original images and the the residual images, left after subtracting the best fitting photometric

model from the original image.

3.1. Light Concentration and Asymmetry

These two parameters are measured following the concepts of Abraham *et al.* (1994) and A95. For the light concentration we use the somewhat different definition :

$$(1) \quad C(\alpha) = \frac{\sum_{r < \alpha \cdot R} I(i,j)}{\sum_{i,j} I(i,j)}$$

where the summation in the denominator is over all image pixels, and that in the numerator is over all pixels (i,j) whose radius r is less than α times the radius of the image, R , which is taken to be the length of the semi-major axis. r is the distance of an image pixel from the image center (corrected for ellipticity). $I(i,j)$ is the intensity of pixel (i,j). The value 0.3 is adopted for the parameter α (the same value was used by A95, although its definition is slightly different there).

The asymmetry parameter is calculated as in A95 by rotating the image by 180° and self-subtracting, and is set equal to the sum of absolute values of pixels in the self-subtracted image over the sum of pixels in the original image :

$$(2) \quad A = \frac{\sum_{i,j} |I(i,j) - I^{rot}(i,j)|}{\sum_{i,j} I(i,j)}$$

3.2. Measuring Texture

Many peculiar galaxies appear “blobby”, while normal galaxies exhibit ordered structures or no structure at all. We require that a measure of the texture take into account the existence of a bright central region in most galaxies, and be sensitive to localised structure. The measure we suggest for HST WFPC2 images is defined as

follows : start by binning the pixel intensities of the raw image into ten linear intensity bins (excluding the lower 5% and upper 2% of pixels, to avoid extreme values). Then examine in turn each of the pixels whose binned intensity is larger than 5 (the upper half of intensities, because it is bright structure that makes the image “blobby”), and denote its distance from the image center (corrected for ellipticity) by d . Since a typical “knot” is no more than 3-4 pixels across, draw a circle of radius 0.5 arcsec (5 pixels) around each such pixel, and consider only points inside the circle whose (ellipticity-corrected) distance from the image center is smaller than d . Now calculate what fraction of these points has a lower binned intensity than that of the pixel of interest. Figure 2 shows a schematic diagram for the process : The solid lines denote intensity contours of an idealised elliptical galaxy and the “X” denotes the current reference pixel. The circle of radius 5 arcsec around it is depicted by the dashed line and the open circles are the pixels we examine. In this idealised case it is obvious that all of those pixels have intensity equal to or higher than that of the reference pixel, and our measure would be zero. This measure should be close to zero for real ellipticals (all pixels closer to the center are necessarily brighter, to within the noise), and should increase as bright localised structures become more dominant. Spiral arms are expected to yield intermediate values, because some pixels closer to the center will be at least as bright (belong to the same arm), while others will be fainter (dust lanes by the side of the arm). Repeating this calculation for all pixels whose binned intensity is larger than 5 and averaging this measure over all of them gives the “blobbiness”, our first parameter.

3.3. Measuring Overall Asymmetries

The asymmetry parameter of A95 is useful, but limited because the detection of asymmetric features is a function of their brightness. This suppresses the detection of galaxies with faint peculiar features (e.g., tidal tails). As a more general approach

we define five isophotal levels for the original image, separated by equal logarithmic intervals. The faintest 15% of image pixels are not considered, because at the faint end pixels form shapes that are very sensitive to noise and inaccurate sky subtraction. The pixels of the image are then divided into five mutually exclusive isophotal groups, and the geometrical center of each of these groups is calculated. The distances between the five centers are worked out and the largest distance, normalised by the image size, is taken as our second parameter (the isophotal center displacement).

3.4. Measuring the Distortion of Shapes

A distortion in the image of a galaxy need not be global. It can happen in the outer regions, say, as a result of weak interactions with nearby galaxies or accretion of gas; or it may only be apparent in the innermost regions, say, after a merger has had time to relax but resulted in a double core. The galaxy may look different at various isophotal levels, even if its isophotes all share roughly the same center. To complement our second parameter, we define the "maximal elliptical envelope" of each isophote as the smallest ellipse containing all the pixels in the isophote. This can be referred to as the "elliptical hull" of the isophote (in analogy with the "convex hull", e.g., Gonzalez and Woods, 1992). The ellipses all share the overall ellipticity and position angle derived for the image as a whole. The distortion of structure at a given isophotal level is then defined as the "filling factor" of its envelope, or more precisely, as the ratio of the number of *isophote* pixels within the envelope to the total number of pixels in it. This ratio approaches 1 for smooth, axisymmetric galaxies and tends to lower values for galaxies with structure. The less ordered the structure, the lower this ratio gets. We found the filling factor of the third (middle) isophote to be the most useful of the five and chose it as our third parameter.

3.5. Quantifying the Nature of Localised Structure

Localised structure is best depicted in the residual images, after the subtraction of the best-fitting smooth model. The major problem is to tell residual structure of one kind (spiral arms) from another (e.g., knots).

In order to quantify the structure we start by binning the intensities of the residual image into 10 logarithmic bins, which are defined ignoring the faintest 5% and the brightest 5% of pixels (thus avoiding extreme values which could be the result of inaccurate profile subtraction). We then define as regions of interest all isolated groups of pixels whose binned intensities are 7 and above, i.e., belonging to the upper 40% of the intensity scale. We reject regions that are either too small (less than 1% of the number of image pixels) or too large (more than 30% of the image). The former are likely to be just noise patches and the latter are unrealistically large structures, which could result from the combined effect of noise and low surface brightness.

For each region we then work out the "skeleton" (Gonzalez and Woods 1992), which can be loosely described as the "backbone" of a consecutive set of points. We briefly describe the algorithm we used in the appendix. In figure 3 we demonstrate these ideas with an example of four stages in the analysis of an image of a grand-design spiral : the original image, the residual (following subtraction of the best fitting smooth model), a map of the detected regions with binned pixel intensities and a map of their skeleta. We measure the ratio of the number of pixels in the skeleton to the number of pixels in the entire region. This ratio is closest to zero for perfectly round shapes, where the skeleton shrinks to a point, and grows towards 1 with the elongation of the shape. It is superior to the axis ratio of a shape (which can be easily obtained from its second moments matrix), because it can follow winding shapes like spiral arms and uncover their true nature. This ratio is then averaged over all regions to get our fourth parameter.

3.6. Independence of the Chosen Parameters of each other

Judging by the definition of our parameters, it may look as if some of them should convey more or less the same information and could become redundant. We check for this possibility by calculating the correlation matrix for our parameters (table 2 below). It is clear that there are no strong linear correlations between any two of them, although the first two appear more correlated than the others.

4. Training an ANN to Classify Normal/Peculiar Galaxies

4.1. Training and Testing the ANN

For an overview of ANNs see Hertz, Krogh and Palmer (1991). Their application to morphological classification of galaxies was discussed in detail elsewhere (Storrie-Lombardi *et al.* 1992; Serra-Ricart *et al.* 1993; Naim *et al.* 1995a; Naim 1995b; and especially Lahav *et al.*, 1996). Briefly, an ANN can be viewed as a non-linear minimising machine which operates in a multi-dimensional space. Nodes are arranged in layers, where input parameters are fed into the nodes of the input layer and the result is read off the output nodes. ANNs which utilise an intermediate (“hidden”) layer between the input and output layers are in general more flexible and perform much better than those without it. The so-called “architecture” of the ANN is the full specification of its nodes and their interconnections. The space in which the ANN operates is spanned by the connection-strengths (“weights”) between the various nodes. The weights are, in effect, the degrees of freedom which are adjusted so as to minimise the error between the actual output reading and the desired output. Training the ANN entails repeated presentations of patterns from a training set, for which the input parameters as well as the desired output values are known. Inputs can be, e.g., morphological parameters and output can be, e.g., morphological type. The training phase ends when a certain stopping criterion is met. Usually one imposes this

criterion in terms of the error of the ANN on a different set of patterns, known as the testing set. It is not recommended to train and test on the same set, since this results in an overfitting of the data and practically “memorising” the particular patterns in that set. If this happens the ANN loses its ability to generalise its “knowledge” and apply it successfully to patterns it has never seen before.

The 978 galaxies in sample 1 are divided into two sets of approximately equal sizes, keeping the ratio of normal to peculiar galaxies the same in both sets. We use one set as a training set and the other as its testing set. Every ANN is run ten times over, each time starting out with a different set of random weights, and its resulting classifications are averaged over the ten runs. This is done because in every run there is the risk of the ANN getting stuck in a local minimum of its error. Using different sets of initial weights and running several times over makes it less likely to get stuck in the same local minimum time after time and one local minimum will stand out against the background of the other runs.

The architecture of the ANN depends first of all on the number of parameters one uses to describe each galaxy. This number determines the number of input nodes. We have six parameters in all :

- Light Concentration, following Abraham *et al.* 1994, A95
- Asymmetry, following A95.
- Blobbiness
- Isophotal Center Displacement.
- Filling Factor of Middle Isophote.
- Ratio of Skeleton size to Region size.

We attempt several combinations of these parameters, as described below. We set the number of hidden layer nodes to three and there are two output nodes, one denoting normal galaxies and the other peculiars. A typical *desired* output vector is either (1,0) or (0,1), stating that that galaxy is of the type whose node is set to 1. The ANN ends up assigning fractional values to the nodes. These output readings can be shown (e.g., Gish 1990; Richard & Lippman 1991) to approximate the *Bayesian a-posteriori* probability for each class given the data, in the limit of very large training sets. The output node with the higher value "wins", and the corresponding type is assigned to that galaxy. We ran three ANNs, which are specified below in terms of their architecture ($N_{input} : N_{hidden} : N_{output}$) and the parameters used as inputs.

1. Using the C-A set of A95 as inputs, architecture 2:3:2
2. Using the 4P set, architecture 4:3:2
3. Using both sets together, architecture 6:3:2

Table 3 shows the resulting classification matrices of these runs, where rows denote eyeball classes and columns denote the resulting classes. Also shown are the "hit rate" (or completeness) and "false alarm rate" (or contamination). The hit rate is defined as the fraction of correct classifications out of the patterns in each eyeball class. The false alarm rate is defined as the fraction of wrong classifications into each eyeball class.

The 4P set appears to give a better result than the C-A set, as could be expected since it utilises four morphological parameters compared with only two in the C-A set. In table 4 we present the results of interchanging the roles of training and testing sets for all three ANNs. The picture remains essentially the same : Using the C-A pair the hit rate over normal galaxies decreases a little, while for the 4P set the same effect is compensated by a higher hit rate for peculiars. This is also what happens when we use all six parameters.

4.2. Improving the Detection of Peculiars

We concentrate here on the ANNs which utilise the 4P set. Table 5 shows the breakdown of successful and unsuccessful classifications of peculiars by the ANN, as a function of the certain/uncertain classification index (see § 2 above). It is obvious that the misclassifications are much more likely when the eyeball classification is uncertain. This means that when one applies the trained ANN to a set of fresh data (e.g., a catalogue of HST images), it will identify most clear cases of peculiarity, but only some of the less certain cases, as one would expect. It is interesting to note that when the ANN is less certain it tends to make more mistakes. Let us define an ANN classification as “uncertain” if the winning class has a probability of less than 0.6. Then only 12% of the successes of the both ANNs are uncertain, while among the misclassifications the fractions rise to 36% for the first ANN and 24% for the second, twice and more.

Although the above statements are reassuring regarding the overall performance of the ANN, one may still wish to do a better job of detecting peculiars, even at a certain price. One way to push the detection level of peculiar galaxies up is to change the proportions of normal and peculiar galaxies in the training set. As was mentioned above, the ANN approximates Bayesian a-posteriori probabilities. These are conditional probabilities for each class given the data, which according to Bayes’ theorem are proportional to the class prior. In other words, if the ANN “knows” that there are many more normal galaxies than peculiars, it will prefer to guess a normal type whenever it is in doubt. If we make the fractions of normals and peculiars equal in the training set we remove the class prior and thus give the peculiars a better chance. This will come at the price of lowering the success rate for normal galaxies and the resulting ANN would not be of use for predicting the overall morphological mix. In Table 6 we show the results of doing this for both of our datasets. The hit rates for peculiars are increased significantly, while those of the normal galaxies drop, as expected.

4.3. Predicting the Morphological Mix

Apart from classifying individual galaxies correctly, it is interesting to see if the ANN is capable of predicting the overall frequencies of peculiar and normal galaxies in a given dataset. This can be done by utilising the ANN probabilities : summing the probabilities assigned to each class over the entire dataset gives a more accurate and robust picture of the morphological mix than counting how many individual galaxies are assigned to each class. The reason is that the actual values of the probabilities convey much more information than the "all or nothing" approach of choosing a winning class and counting whole numbers. In effect, summing up probabilities is not subject to the "round-off" errors that arise when one sums integer numbers. The picture is not so simple, though : The ANN approximates the conditional probability of each class given the data, which depends on the class prior probability. As a result, if one presents the ANN with a set of galaxies in which the fractions of normals and peculiars are very different from their fractions in the training sets, the ANN will not give the correct morphological mix. The practical implication is that so long as our training sets have *roughly* the correct mix, we can use the ANN to predict the mix in any large dataset. This is the single most important requirement, and a very natural one : The training set must represent the "true" world faithfully. A supervised ANN can therefore be trained to mimic the human decision process (Naim *et al.* 1995a) and thus save much effort and time. The trained ANN is a parametric, non-linear classifier, and is not limited to a small number of parameters. In this respect it is superior to linear discriminatory analysis, and is more repeatable than eyeball classification.

Even if the training set contains roughly the correct mix of normals and peculiars, it is unlikely to give *exactly* the same mix. As can be seen in the top panel of figure 4, when one presents the trained ANN with different fractions of peculiars its predicted fraction changes almost linearly with the actual fraction, but this linear relation has a slope much flatter than the desired value of 1. We produced figure 4 by specifying nine different fractions of peculiars, ranging from 20% to 60% in steps of 5%. For each

of these values we select four independent subsets of 40 galaxies each from the testing set, and sum the probabilities given by the ANN to get the predicted fractions for each of the four subsets. We then average the ANN predictions over the four datasets and work out their standard deviations, which are depicted by the error bars in the figure. Also shown in the top panel of figure 4 is the straight line of slope 1 which represents the desired relation between the predicted and the actual fractions of peculiars.

The question is then how to correct the mix predicted by the ANN to get a more realistic prediction. Since the ANN prediction varies almost linearly with the true fraction, the simplest thing to do is fit a straight line to the predicted fractions and use its slope and zero crossing to correct the prediction. The bottom panel of figure 4 shows the result, and the straight line of slope 1 is again plotted just to guide the eye. The error bars are estimated from the derived errors in the slope and zero-crossing of the fitted line. This procedure gives us an estimate of the error in predicting the morphological mix, and can be used for any set of galaxies with a peculiar fraction between 20% and 60%.

5. Limits of Applicability

We now turn to study the accuracy of ANN classifications as a function of various limiting quantities. In figure 5 we show three histograms describing the hit rates of the ANN as a function of magnitude, signal-to-noise ratio and image size. Magnitudes are isophotal (Ratnatunga *et al.*, *in preparation*). Signal-to-noise ratios are integrated over all pixels associated with the image (as determined by the object detection algorithm), for which the individual ratio is larger than 1. This limit is imposed in order to avoid inclusion of large patches of sky in the image. Image size is the number of pixels whose intensity is at least 5σ above sky, i.e., the bright pixels of the image. The success rate for normal galaxies drops almost steadily as one goes fainter and as the ratio of signal-to-noise decreases. A similar trend exists when the number of bright

pixels decreases. However, the picture is less clear with respect to the peculiar galaxies : The trend with magnitude is "bumpy" as is the trend with signal-to-noise, though the dependence on the number of bright pixels appears more stable. We conclude that our analysis does not break down sharply at any point, although if one's concern is mainly with the identification of peculiars we would advise keeping the signal-to-noise ratio above 180 and the number of bright pixels above 50.

6. The Distribution of Bulge-to-Disk Ratios

We now turn to apply the trained ANN to the larger sample 2, which was not classified by eye. This sample contains 2319 images and includes stars as well as galaxies. A quantitative criterion that will allow us to reject stars without resorting to eyeball classification is required. We use the maximum likelihood software (Ratnatunga *et al.*, *in preparation*) to fit a smooth photometric model to each galaxy image. The model has 10 degrees of freedom, among which is the log of the effective half light radius. This parameter is expected to be very small for stars and larger for galaxies. We test this expectation in figure 6, where we show two histograms depicting the distribution of half light radii in the eyeballed sample 1. The dashed line depicts images which were eyeballed as either stars or point sources, and the solid line depicts those that were deemed galaxies. There is a sharp distinction between the two populations at a half light radius of roughly 0.1 arcsec, which corresponds to a single pixel in WFPC2 images. This value is a function of magnitude, and compact, high redshift galaxies may be excluded. However, we do not have any other means for removing stars from our sample, and regardless of the true nature of an object, if its half light radius is less than one pixel it contains very little morphological information for our analysis. We therefore reject from sample 2 those images whose best fitted half light radius is less than this value. The number of rejected images is 320, and we are left with 1999 galaxies in this sample. These are then classified using the trained

ANN.

One of the parameters fitted by the maximum likelihood algorithm is the bulge-to-total ratio, which is defined as the ratio of light in the fitted bulge component to the sum of the light in the fitted bulge and disk components (integrated to infinity for both). This B/T ratio is a quantitative measure of the dominance of the bulge in the underlying photometric model, and by construction is less susceptible to bright overlying features than is the cruder light concentration. The software makes a decision, based on the signal-to-noise ratio of the image, whether to fit a full bulge+disk model or to fit only a pure bulge or a pure disk. In these latter cases the B/T ratio is automatically fixed at 1 or 0 (respectively). In figure 7 we plot the Light Concentration index against the B/T ratio, and the large numbers of points at B/T values of 0 and 1 are a testimony of the significant fractions of images that were fitted as either pure bulges or pure disks. The two quantities are not very correlated, which is surprising. Since the B/T has been checked for simulated images and gave very good results (Ratnatunga *et al.*, *in preparation*), we conclude that the light concentration index is too sensitive to structure superimposed on the underlying smooth model. We therefore concentrate in what follows on the B/T ratio as the primary indicator of bulge dominance. In figure 8 we show the distribution of the B/T ratios among normal and peculiar galaxies, as classified by the ANN. The plot includes galaxies for which the estimated error in the B/T ratio was less than 0.1 (the width of a single bin in the histograms). This excludes 122 out of the 1999 galaxies. It is clear that the fraction of disk dominated peculiars is larger than the corresponding fraction for normal galaxies. Nevertheless, about 17% of all peculiars have a B/T ratio larger than 0.5, which we take as “bulge dominated”. While this is less than the corresponding 23% among normals, it still implies a significant population.

7. Discussion

The frequencies of various morphological types that are quoted in the literature are almost invariably estimated on the basis of eyeball classifications. As a result it is difficult to compare work done by different observers because they have different criteria for peculiarity. A95 made the crucial step of introducing a *quantitative* criterion, but as shown above it gives only a low hit rate for peculiars, together with a significant contamination by normal galaxies. The confusion between normal and peculiar galaxies can be seen in figures 5 and 6 of their paper, where one also sees several peculiars lying in the region dominated by ellipticals. Their use of the light-concentration index as a second parameter precludes bulge dominated peculiar galaxies from the outset. It might be better to define peculiarity on the basis of shape alone, without any reference to the distribution of light.

We therefore adopt a purely morphological approach, concentrating on the features that make a galaxy appear peculiar to the eye. This then gives us the freedom to define the population of peculiars on a morphological basis and examine the distribution of bulge-to-disk ratios in this population separately. As we show above, there is indeed a population of bulge-dominated peculiars. This population probably corresponds to the “blue nucleated galaxies” (BNGs) found in the Canada-France Redshift Survey (CFRS, Schade *et al.* 1995; Schade *et al.* 1996), although this correspondence is still to be confirmed. Unlike CFRS we do not have redshifts for the galaxies in our sample but our imaging is much better, coming from HST. The success of fitting a bulge photometric model depends strongly on the point spread function, and therefore it is not obvious that ground based images deemed bulge dominated will maintain this quality when imaged by HST (see Ratnatunga *et al.*, *in preparation* for a fuller discussion of this point).

We apply the ANNs trained using the 4P set to a collection of 1999 galaxies taken from the other 18 fields of the Groth-Westphal strip (Groth *et al.* 1995). Summing

up the probabilities for peculiars over this entire set and inverting to get the true frequency of peculiars at moderate redshifts, we find this frequency to be $35 \pm 15\%$. The error we obtain is the first to date to rely on statistical estimates rather than on the much cruder estimate of eyeball classification errors for individual galaxies. The fact that the error bar is large is a reflection of the uncertainties involved in the entire process.

It is quite clear now that so long as the automated procedure relies on eyeball classifications it will be partly subjective and difficult to standardise. What is called for at this stage is a set of quantitative parameters that adequately describe the appearance of galaxies. In this paper we provide such a set. Once the parameter space is fixed, one way to proceed is to look for correlations with other sources of information (e.g., colours, luminosities), and examine whether in this space the locus of galaxies of, e.g., a certain colour is significantly different that the locus of galaxies of a different colour.

Morphological classification is a good starting point for studying galaxy evolution, by virtue of the large numbers of available images. However, it can only serve as a first step, because galaxy shapes form a continuum rather than break down to separate groups. In addition, the classes one defines by eye might not always have a one-to-one correlation with the dynamics and chemistry of galaxies. In this paper we use morphology as tool for singling out interesting galaxies for more detailed studies. The next logical step is to examine where different populations of galaxies reside in the space of our morphological parameters, without recourse to any kind of classification. Work along these lines is currently in progress (Naim *et al.*, *in preparation*). Hopefully, once large quantities of physical data (e.g., spectra, rotation curves) are available for these galaxies, we will be able to quantify and understand galaxy evolution much better.

ACKNOWLEDGEMENTS

We would like to thank Ofer Lahav for statistical insight and Brian Ripley for allowing us to use his ANN code. Stefano Casertano and Myungshin Im read the manuscript and raised valuable points and Eric Ostrander’s contribution to the MDS pipeline processing of the images was invaluable. The referee made useful comments and we thank him for helping us make this paper more readable. This research was supported by funding from the HST Medium Deep Survey under GO grants p2684 *et seq.*

APPENDIX : Algorithm for Calculating the Skeleton of an Image

The following algorithm appears in Gonzalez & Woods (1992) and was adopted by us for calculating the skeleta of galaxy features. This algorithm is suitable for skeletoning binary regions, i.e., regions in which each pixel is either part of the feature whose skeleton we seek (value 1) or does not belong to it at all (value 0). No reference is made to the actual intensity of the pixels.

Denote a pixel in the image by p_1 and its nearest eight neighbours by p_2, \dots, p_9 , starting with the one directly above it and going clockwise around it (figure 9). Define as contour points pixels whose value is 1, with at least one neighbour whose value is zero. The skeletoning process is iterative and consists of repeating a set of two steps. In each step we examine value 1 pixels and those that comply with a given set of criteria are flagged for deletion. The values of pixels flagged for deletion are all changed to 0 at the end of each step. The process stops once no more pixels are flagged for deletion.

In step 1 of each iteration a pixel p_1 is flagged for deletion if it fulfills all of the following requirements :

- the number of value 1 neighbours is in the range $[2, 6]$

- the number of changes from value 0 to value 1, as one goes clockwise around p_1 , is 1.
- the value of at least one of p_2, p_4 and p_6 is zero.
- the value of at least one of p_4, p_6 and p_8 is zero.

In step 2 the first two requirements remain unchanged, but the last two are modified as follows :

- the value of at least one of p_2, p_4 and p_8 is zero.
- the value of at least one of p_2, p_6 and p_8 is zero.

This procedure is somewhat dependent on the order of the steps and the resolution of the image (a small number of pixels will normally imply a highly discretised contour and consequently a less dependable skeleton).

Table 1: Breakdown of Morphological Eyeball Classifications in I and V bands.

I / V	E/S0	Se	S1	P1	P2	Total
E/S0	46	21	5	0	0	72
Se	12	158	80	37	28	315
S1	0	17	174	46	48	285
P1	0	9	10	91	32	142
P2	0	1	13	16	134	164
Total	58	206	282	190	242	

Table 2: Correlation Matrix for the Parameters of the 4P Set.

	Blobb- iness	Iso. Disp.	Iso. Fill.	Skel. Ratio
Blobbiness	1.00	-0.47	0.14	-0.21
Iso. Disp.	-0.47	1.00	0.24	-0.02
Iso. Fill.	0.14	0.24	1.00	-0.22
Skel. Ratio	-0.21	-0.02	-0.22	1.00

Table 3: Results of ANN trained on set 1 and tested on set 2.

Using the C-A Pair (Light Concentration and Asymmetry)

	ANN	ANN	Hit	False
	Normal	Peculiar	Rate	Alarm
Eyeball Normal	316	19	94%	28 %
Eyeball Peculiar	120	34	22%	36 %

Using the 4P Set

	ANN	ANN	Hit	False
	Normal	Peculiar	Rate	Alarm
Eyeball Normal	291	44	87%	23 %
Eyeball Peculiar	87	67	44%	40 %

Using All Six Parameters

	ANN	ANN	Hit	False
	Normal	Peculiar	Rate	Alarm
Eyeball Normal	299	36	89%	22 %
Eyeball Peculiar	83	71	46%	34 %

Table 4: Results of ANN trained on set 2 and tested on set 1.

Using the C-A Pair

	ANN	ANN	Hit	False
	Normal	Peculiar	Rate	Alarm
Eyeball Normal	307	28	92%	28 %
Eyeball Peculiar	117	36	24%	44 %

Using the 4P Set

	ANN	ANN	Hit	False
	Normal	Peculiar	Rate	Alarm
Eyeball Normal	305	30	91%	22 %
Eyeball Peculiar	86	67	44%	31 %

Using All Six Parameters

	ANN	ANN	Hit	False
	Normal	Peculiar	Rate	Alarm
Eyeball Normal	304	31	91%	21 %
Eyeball Peculiar	80	73	48%	30 %

Table 5: Breakdown of ANN Successes and Failures in classifying Peculiars, as a function of the degree of Certainty in Eyeball Classifications.

For the ANN trained on set 1.

	Eyeball Certain	Eyeball Uncertain
ANN Sucesses	48	19
ANN Failures	40	47

For the ANN trained on set 2.

	Eyeball Certain	Eyeball Uncertain
ANN Sucesses	52	15
ANN Failures	35	51

Table 6: Results of ANN Trained on Equal Numbers of Normals and Peculiars.
Compare with tables 3 and 4.

Training on Set 1

	ANN	ANN	Hit	False
	Normal	Peculiar	Rate	Alarm
Eyeball Normal	108	46	70%	30 %
Eyeball Peculiar	46	108	70%	30 %

Training on Set 2

	ANN	ANN	Hit	False
	Normal	Peculiar	Rate	Alarm
Eyeball Normal	95	59	62%	27 %
Eyeball Peculiar	35	118	77%	33 %

REFERENCES

- Abraham, R.G., Valdes, F., Yee, H.K.C. & van den Bergh, S., 1994, *Ap.J.*, **432**, 75.
- Abraham, R.G., van den Bergh, S., Glazebrook, K., Ellis, R.S., Santiago, B.X., Surma, P. & Griffiths, R.E., 1995, *Ap.J.Supp.*, *in press*.
- Arp, H.C., *Atlas of Peculiar Galaxies*, 1966.
- Cowie, L.L., Hu, E.M. & Songaila, A., 1995, *Nature*, **377**, 603.
- Dalcanton, J.J. & Sackett, S.A., 1996, *to appear in Ap.J. Lett.*
- de Vaucouleurs, G., 1959, in: Flügge, S. (ed.), *Handbuch der Physik*, **53**, 275, Berlin: Springer-Verlag.
- Driver, S.P., Windhorst, R.A. & Griffiths, R.E., 1995, *Ap.J.*, **453**, 48.
- Glazebrook, K., Ellis, R.S., Santiago, B.X. & Griffiths, R.E., 1995, *Mon. Not. R. Astr. Soc.*, **275**, L19.
- Gonzalez, R.C. & Woods, R.E., 1992, *Digital Image Processing*, New-York : Addison-Wesley.
- Griffiths, R.E., Casertano, S., Ratnatunga, K.U., Neuschaefer, L.W., Ellis, R.S., Gilmore, G.F., Glazebrook, K., Santiago, B., Huchra, J.P., Windhorst, W.A., Pascarelle, S.M., Green, R.F., Illingworth, G.D., Koo, D.C. & Tyson, A.J., 1994, *Ap.J.*, **435**, L19.
- Groth, E. J., Kristian, J. A., Lynds, R., O’Neil, E. J., Balsano, R., Rhodes, J., 1994, *BAAS*, **26**, 1403
- Hertz, J., Krogh, A., & Palmer, R.G., 1991, *Introduction to the Theory of Neural Computation*, Addison-Wesley, California.
- Hubble, E., 1936, *The Realm of Nebulae*, New Haven: Yale University Press.

Lahav, O. & Naim, A., 1996, *submitted to M.N.R.A.S.*

Lahav, O., Naim, A., Sodr e Jr., L. & Storrie-Lombardi, M.C., 1996, *submitted to M.N.R.A.S.*

Naim, A., Lahav, O., Sodr e Jr., L. & Storrie-Lombardi, M.C., 1995a, *M.N.R.A.S.*, **275**, 567.

Naim, A., 1995b, Ph.D. Thesis, Cambridge University.

Ratnatunga, K.U., Griffiths, R.E. & Ostrander, E.J., 1996, *Ap.J.*, submitted.

Sandage, A.R., 1961, *The Hubble Atlas of Galaxies*, Washington: Carnegie Institute of Washington.

Schade, D., Lilly, S.J., Crampton, D., Hammer, F., Le F evre, O., & Tresse, L., 1995, *Ap.J.*, 451, L1.

Schade, D., Lilly, S.J., Le F evre, O., Hammer, F. & Crampton, D., 1996, *Ap.J.*, 464, 79.

Serra-Ricart, M., Calbert, X., Garrido, L. & Gaitan, V., 1993, *A.J.*, **106**, 1685.

Storrie-Lombardi, M.C., Lahav, O., Sodr e Jr., L. & Storrie-Lombardi, L.J., 1992, *M.N.R.A.S.*, **259**, 8p.

van den Bergh, S., 1976, *Ap.J.*, **206**, 883.

Figure Captions :

Figure 1 : twelve Galaxies from our Sample 1. The top Nine were Classified as Peculiars and the Bottom Three as Normal Galaxies.

Figure 2 : derivation of the Blobbiness Parameter : Idealised Elliptical Case.

Figure 3 : skeletoning of a Grand-Design Spiral. Top Left : The Original Image; Top Right : The Residual Image; Bottom Left : Detected Regions; Bottom Right : Skeleta of the Regions.

Figure 4 : ANN Prediction of the Morphological Mix vs. the True Mix. Top : Before applying correction; Bottom : After applying correction.

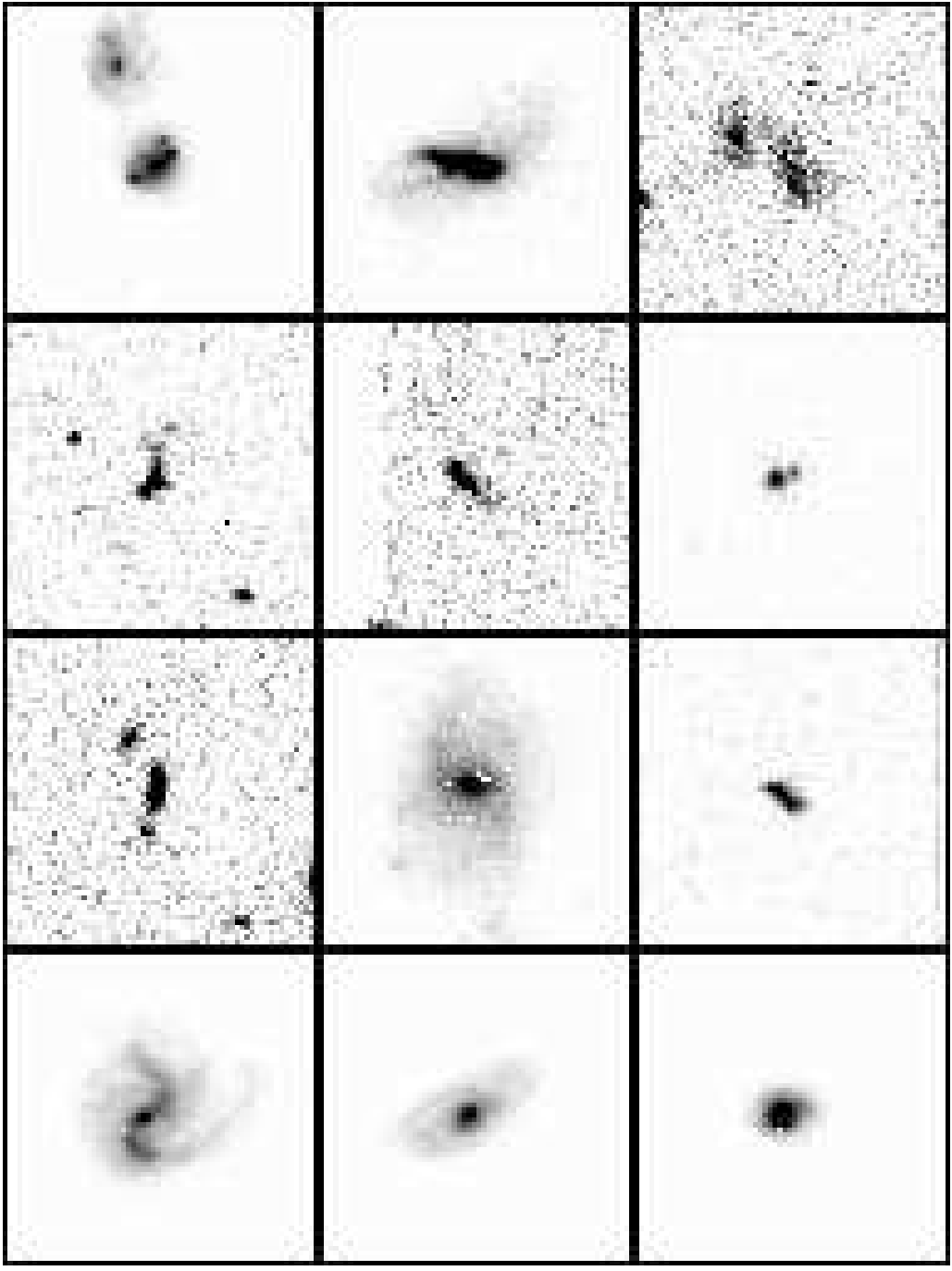
Figure 5 : the Dependence of ANN Success Rates on Magnitude (Top Left), Integrated Signal-to-Noise Ratio (Top Right), and Image Size (Bottom Right). Normal galaxies are depicted by the solid line, Peculiars by the dashed line.

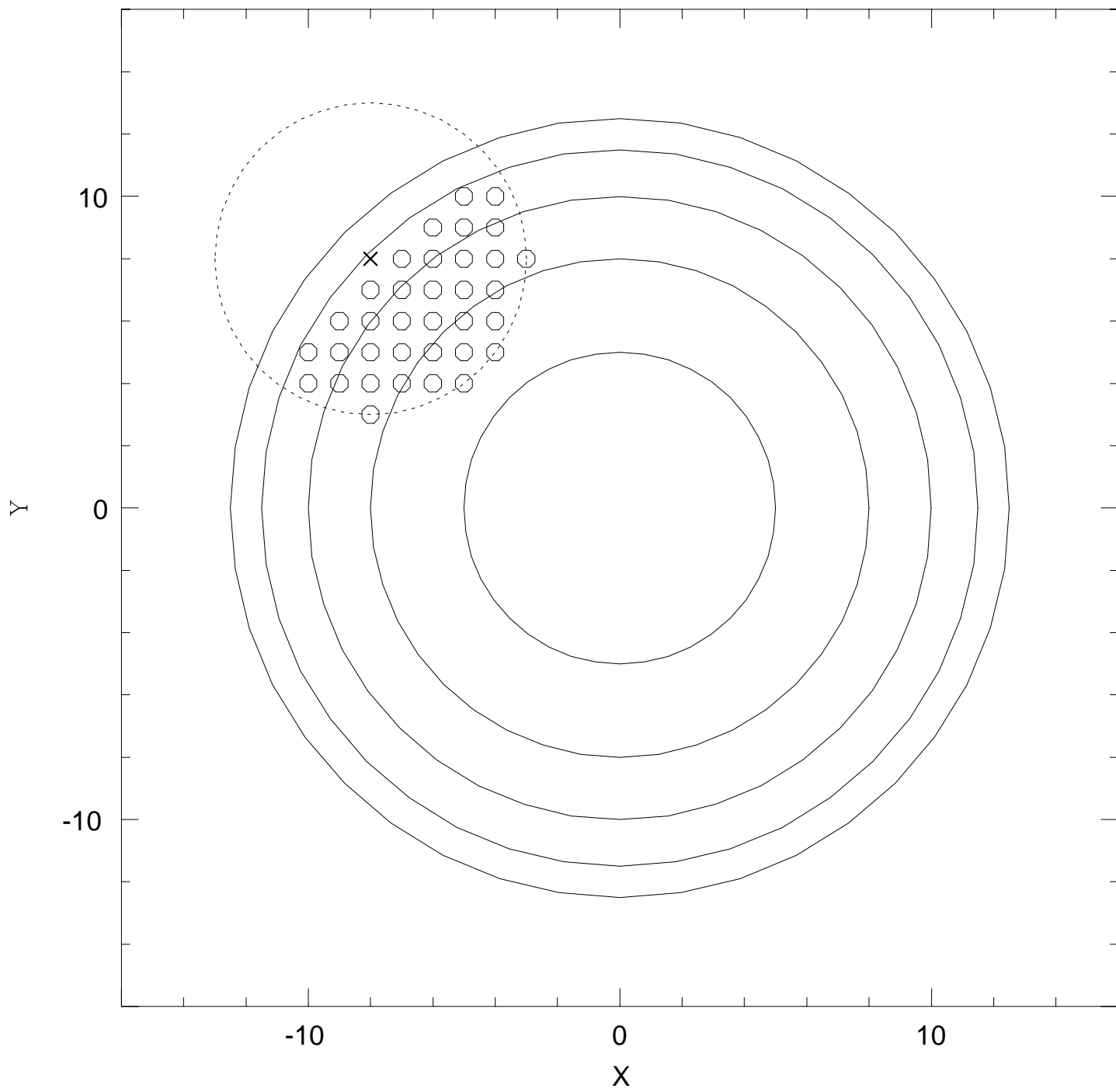
Figure 6 : the Distributions of Fitted Half Light Radii for Eyeball Point Sources and Eyeball Galaxies.

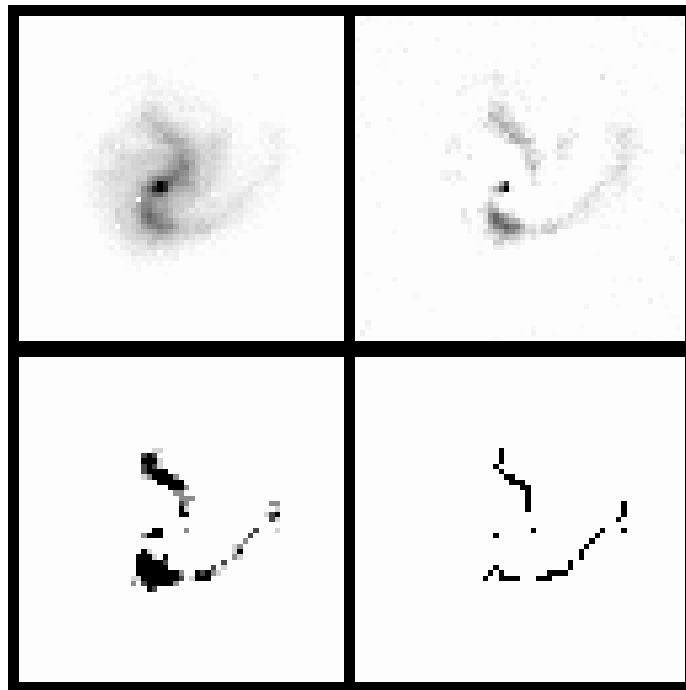
Figure 7 : the Lack of Correlation between Light Concentration and the Maximum Likelihood B/T Ratio.

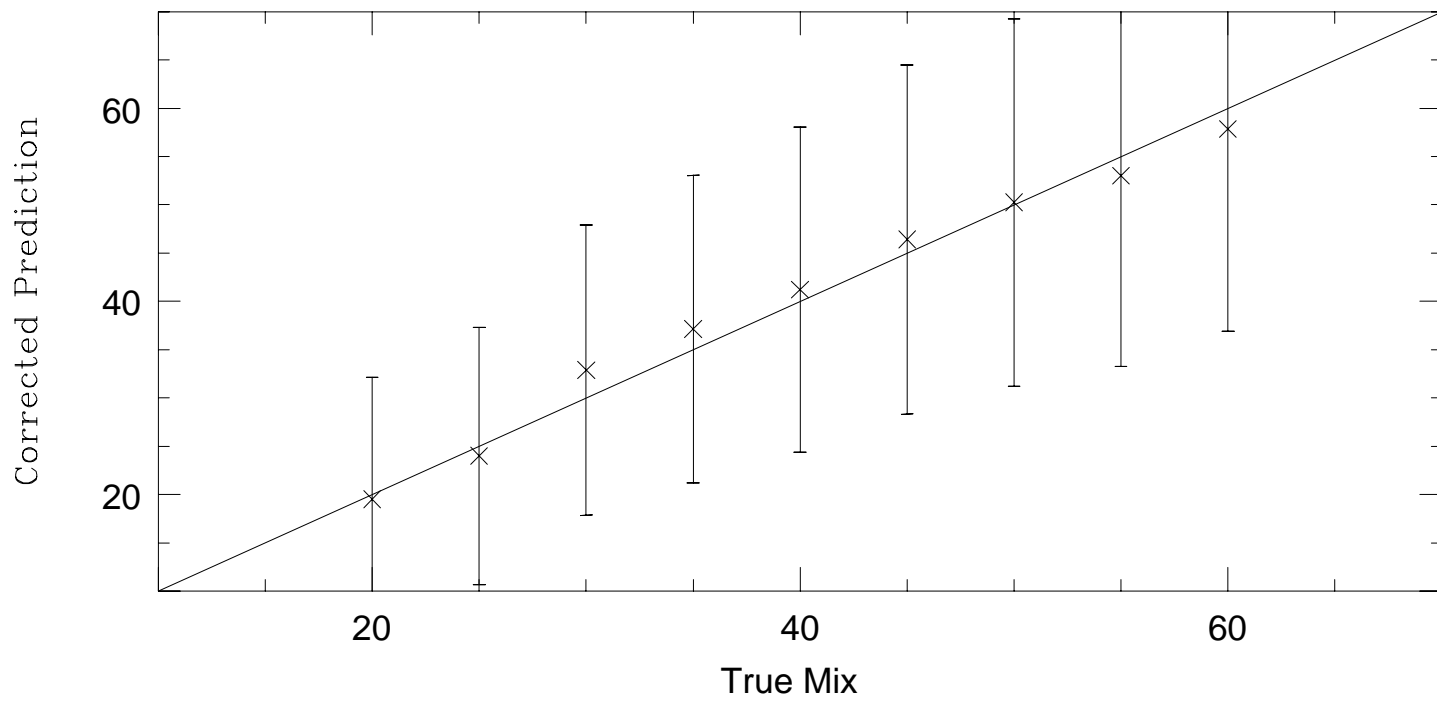
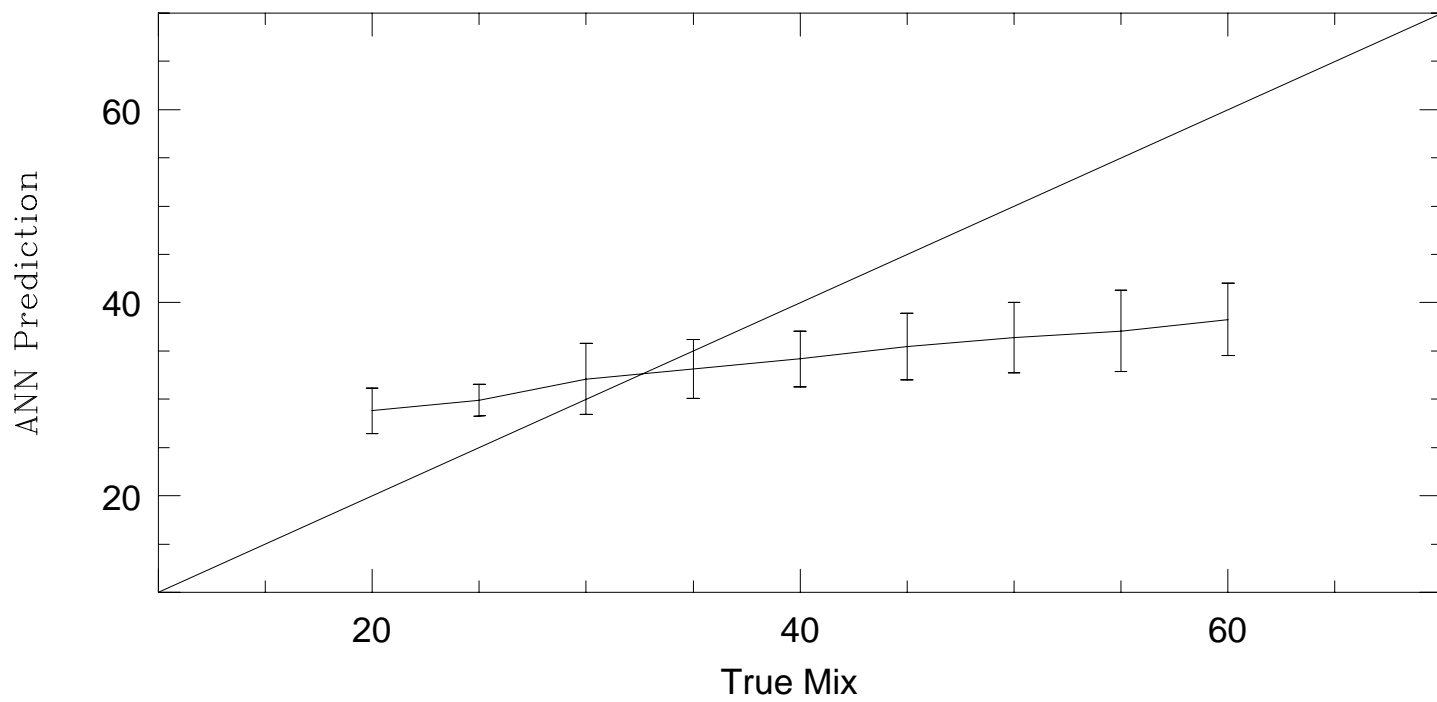
Figure 8 : the Distributions of B/T Ratios among Normal and Peculiar Galaxies.

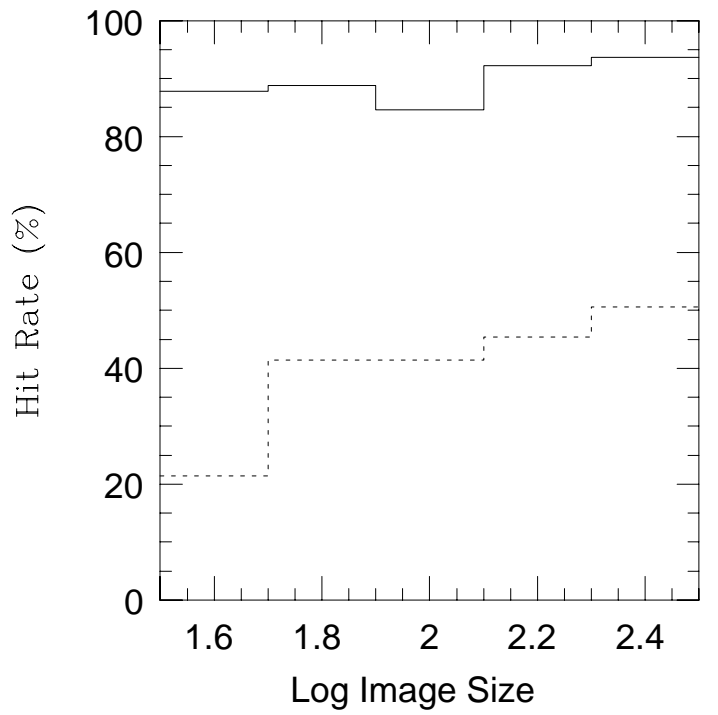
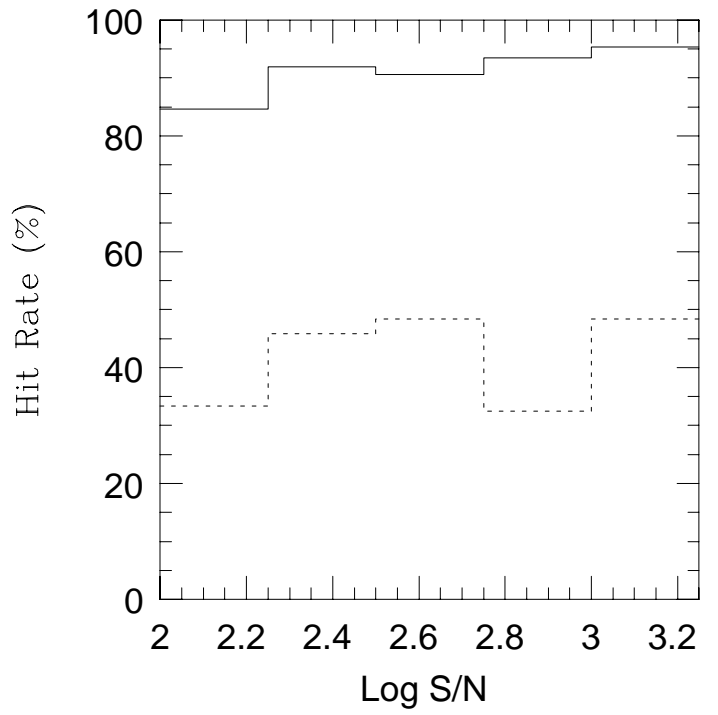
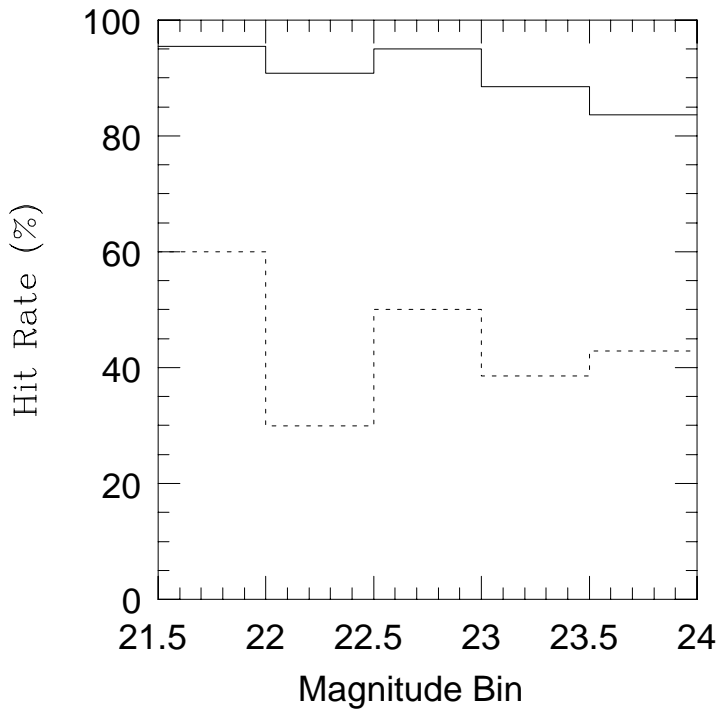
Figure 9 : the notation used for the neighbours of a given pixel p_1 in the skeletoning algorithm.

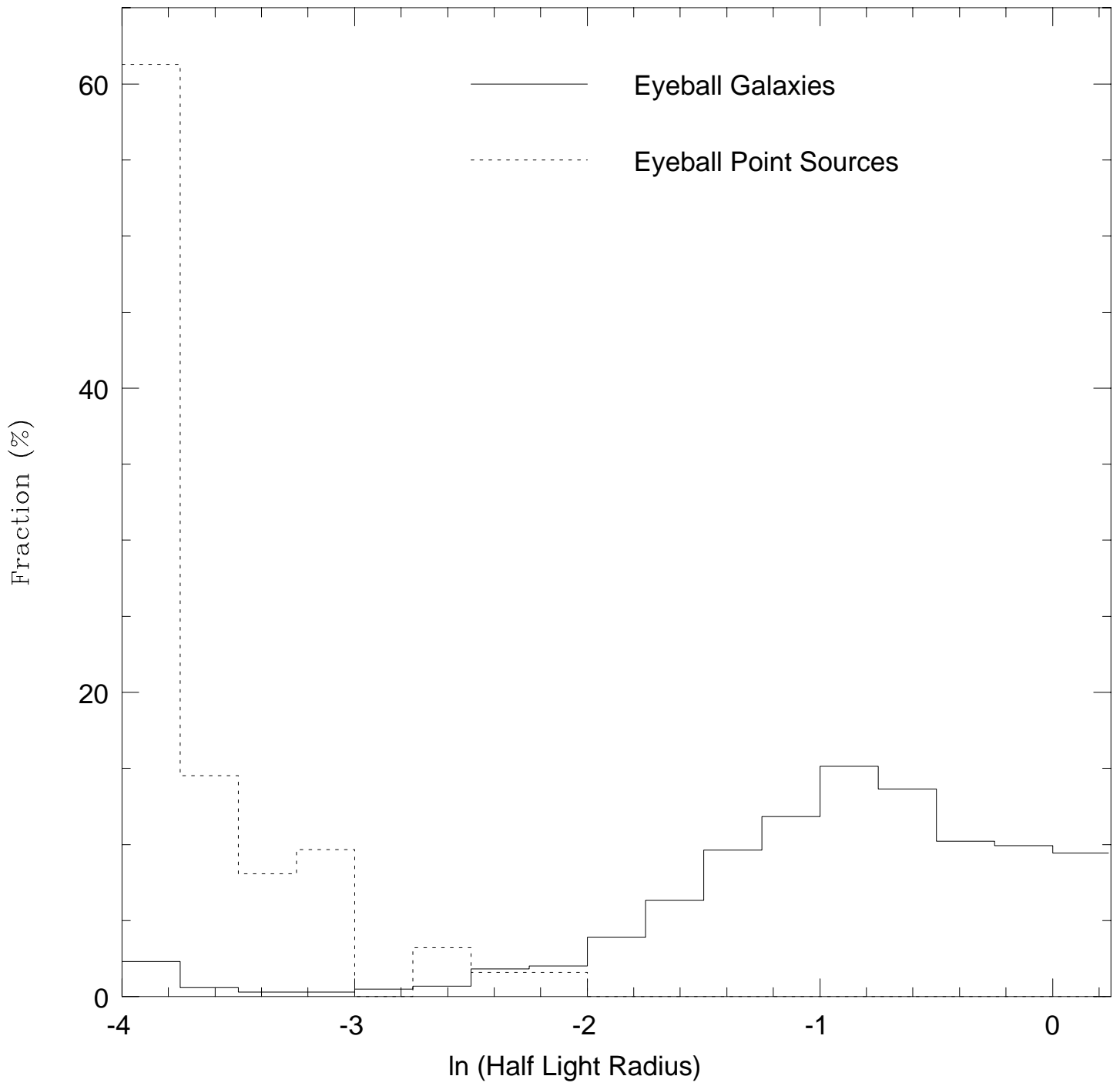


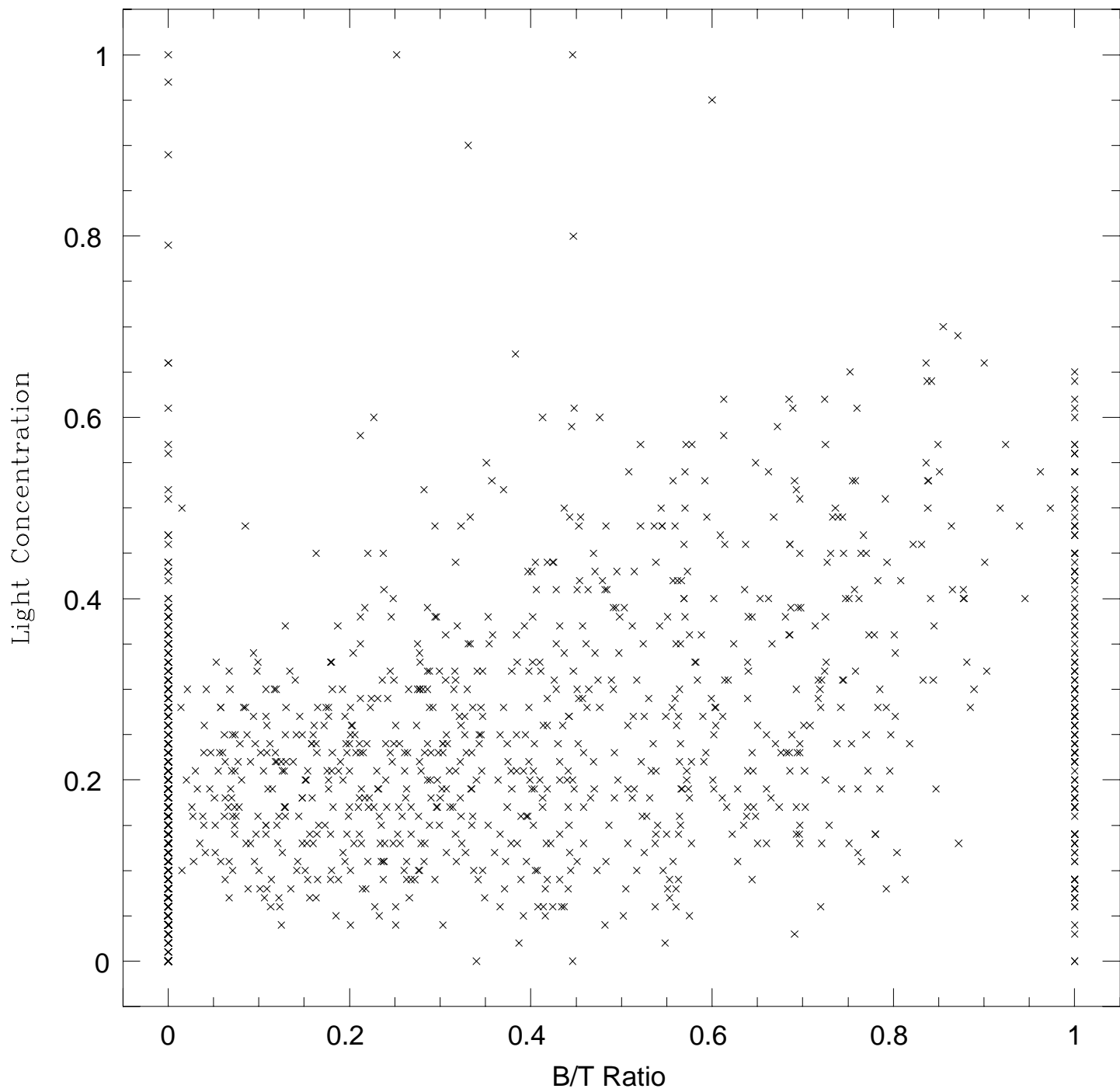


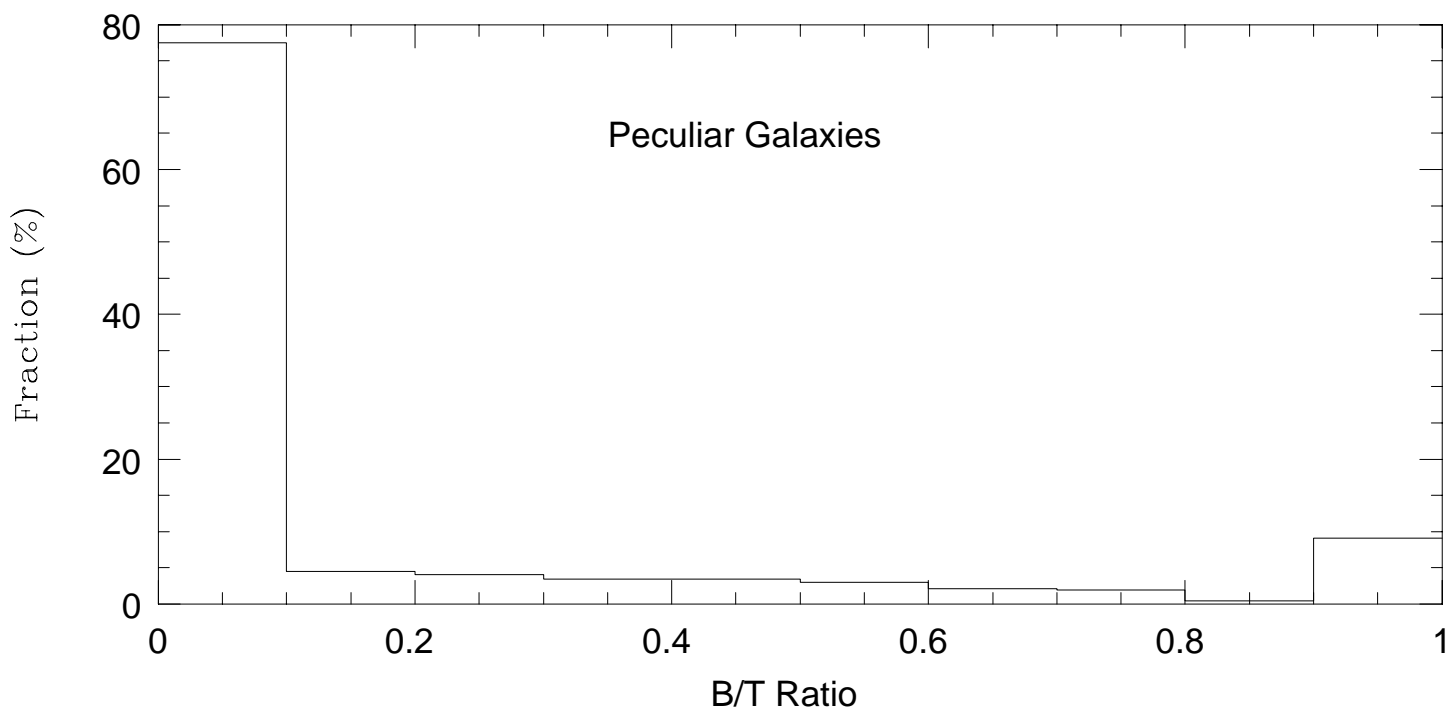
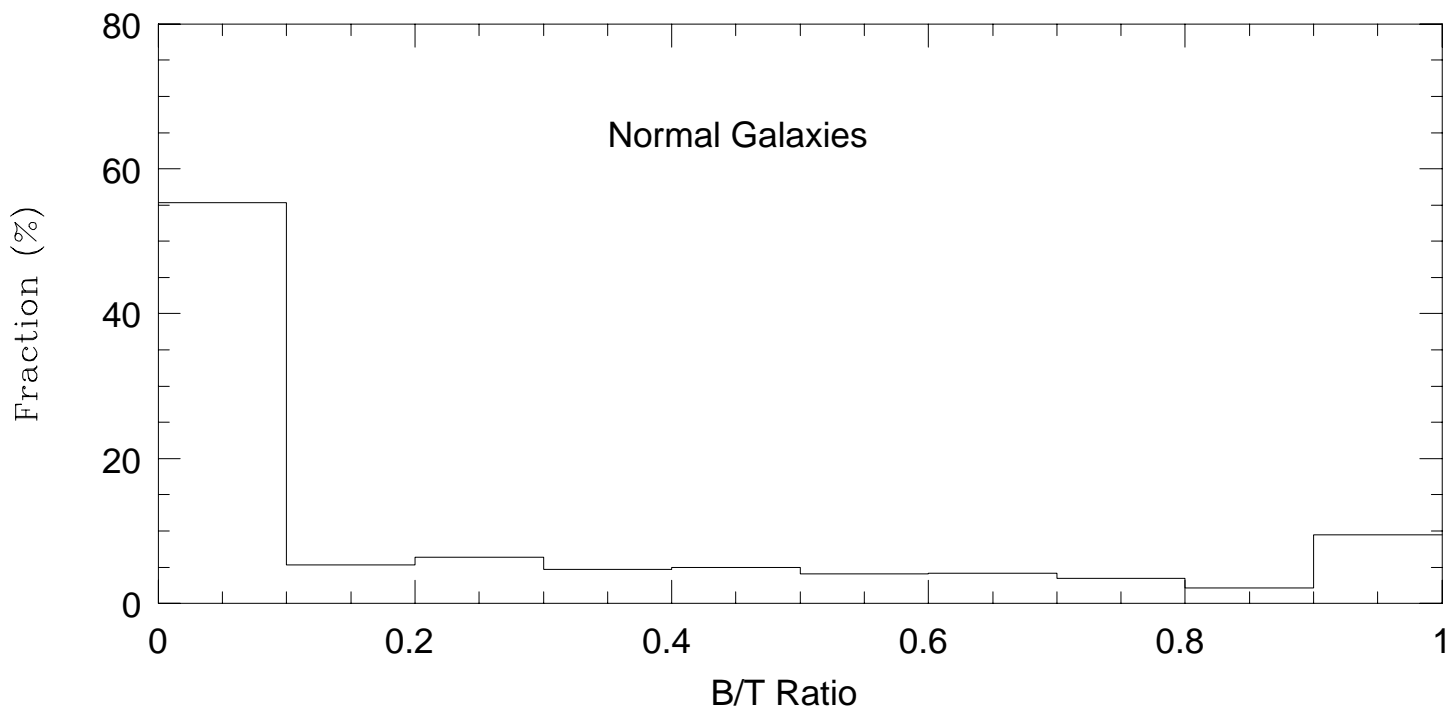












P9	P2	P3
P8	P1	P4
P7	P6	P5